Hindawi
Journal of Nanomaterials
Volume 2019, Article ID 9151979, 9 pages
https://doi.org/10.1155/2019/9151979

Research Article

Preparation of $Ga_{0.25}Zn_{4.67}S_{5.08}$ Microsphere by Ultrasonic Spray Pyrolysis and Its Photocatalytic Disinfection Performance under Visible Light

Tuo Yan,[1,2] **Jianhui Huang**,[2,3] **Jinhong Bi**,[1] **Liyan Xie**,[2,4] **and Huimin Huang**[1]

[1]*College of Environment & Resources, Fuzhou University, Fuzhou 350108, China*
[2]*College of Environmental & Biological Engineering, Putian University, Putian 351100, China*
[3]*Fujian Provincial Key Laboratory of Ecology-Toxicological Effects & Control for Emerging Contaminants, Putian 351100, China*
[4]*Key Laboratory of Ecological Environment and Information Atlas, Fujian Provincial University, Putian 351100, China*

Correspondence should be addressed to Jianhui Huang; owenhuang95@163.com

Received 2 September 2019; Accepted 2 December 2019; Published 23 December 2019

Academic Editor: Sesha Srinivasan

The $Ga_{0.25}Zn_{4.67}S_{5.08}$ catalysts were prepared by ultrasonic spray pyrolysis with thiourea as a precursor. The crystal structure, optical properties, specific surface area, chemical composition, surface morphology, and internal structure of the prepared samples were characterized by XRD, UV-Vis DRS, BET, XPS, SEM, and TEM, respectively. The disinfection performance and the main active species of the synthesized catalysts under visible light irradiation were investigated with *E. coli* K12. The study results indicate that $Ga_{0.25}Zn_{4.67}S_{5.08}$ prepared at 400°C exhibited the best antibacterial performance with complete kill of *E. coli* K12 within 4 h. The antibacterial performance of the prepared sample is also higher than that prepared by the hydrothermal method. The result of the radical trapping experiment indicates that the photogenerated holes play a dominant role in the disinfection process.

1. Introduction

Various pathogenic bacteria living in waters have always been the greatest threat to human health. The statistic data show that millions of people were disabled or die because of bacteria every year [1]. Traditional sterilization techniques include chemical sterilization and ultraviolet (UV) disinfection. Among them, the chemical disinfection method uses strong oxidants such as liquid chlorine, sodium hypochlorite, chloramine, chlorine dioxide, or ozone, which has an efficient sterilization effect and effectively protects people's drinking water safety. However, liquid chlorine and sodium hypochlorite can increase the risk of disinfection by-product (DBP) formation [2, 3]. Chloramine disinfection may form carcinogenic nitrosamines and nitrite substances by reacting with nitrates and inorganic salts. Chlorine dioxide and chlorite may be produced during chlorine dioxide disinfection, causing blood erythrocyte damage and limiting oxygen transport [4]. Ozone disinfection has high energy consumption and may oxide some aqueous organic substances to form carboxylic acids, formaldehyde, ketones, and other carcinogenic and genetic toxic by-products [5].

The UV disinfection method can rapidly achieve the effect of sterilization and disinfection by damaging the molecular structure of microbial DNA or RNA without producing DBPs [6]. However, some bacteria, such as spores, fungal spores, Mycobacterium tuberculosis, and Bacillus subtilis, are highly resistant to ultraviolet light. In addition, some bacteria have the ability of self-repair or resurrection, so the sterilization is not durable. These problems limit the further popularization of UV disinfection [7]. Except for those mentioned above, the heavy metal ions such as Ag^+ were also reported to have superior ability in cell killing; however, the high toxicity limits their application in disinfection [8].

Therefore, it is urgent to develop an economical, safe, and efficient disinfection technology for microbial inactivation in water [9].

In recent years, photocatalytic sterilization technology with photocatalyst as the core has attracted more and more attention due to its advantages of direct utilization and conversion of sunlight, high efficiency, stability, and no by-product formation [10]. Some traditional semiconductor materials such as TiO_2 and ZnS have the ability of photocatalytic sterilization. However, these semiconductors are hampered by a large intrinsic band gap. Based on the above limitation, enormous efforts, such as doping and heterojunction construction, have been investigated to broaden the visible light response [11–14], but the photocatalytic efficiency was still not obviously enhanced, which greatly limited their practical application. Therefore, it is imperative to develop a new type of high-efficiency photocatalyst to make up for the shortcomings of traditional materials. Recent series of studies have shown that ternary sulfides such as Cu_3SbS_3 [15], $ZnIn_2S_4$ [16], $Cu_2Mo_6S_8$ [17], and CuS_xSe_{1-x} [18] are highly attractive due to their low cost, excellent electrical properties, and nonlinear optical properties. Particularly, their physicochemical properties can be facile regulated by adjusting the composition of each element, making them stand out among many new photocatalysts [19]. The literature reports that Ga_2S_3 is an effective optoelectronic material; however, its wide band gap (E_g = 3.4 eV) limits the application of visible light [20]. Therefore, a new ternary sulfide photocatalyst with an adjustable and optimized band structure can be obtained by introducing new metal elements in the crystal phase structure of Ga_2S_3.

At present, the preparation methods of ternary sulfides mainly include the hydrothermal method [21], electrochemical method [22], and microwave-assisted method [23]. Most of these methods need high temperature, high pressure, or external template to control the morphology; thus, it is difficult to be widely used. In recent years, it has been reported that the ultrasonic spray pyrolysis (USP), which can be carried out under ambient pressure with no template, serves as a novel preparation method for photocatalyst. It mainly includes atomization of the solution by means of an atomizer and the physicochemical reaction of the droplets under heating conditions [24]. The catalyst particles with a high specific surface can be obtained by USP, and the photocatalytic efficiency can be significantly improved compared to conventional preparation methods.

In this study, a novel ternary sulfide photocatalyst $Ga_{0.25}Zn_{4.67}S_{5.08}$ was prepared using USP. The effect of reaction conditions on the $Ga_{0.25}Zn_{4.67}S_{5.08}$ was studied, and their photocatalytic activities were evaluated using bacterial disinfection under visible light irradiation.

2. Experimental Section

2.1. Catalyst Preparation. The $Ga_{0.25}Zn_{4.67}S_{5.08}$ photocatalyst was prepared by a USP method. All chemicals used for synthesis were of analytical grade and used without further purification. In a typical process, 0.297 g $Ga(NO_3)_3{\cdot}XH_2O$, 0.511 g $Zn(NO_3)_3{\cdot}6H_2O$, and 0.761 g CH_4N_2S were added into 150 mL distilled water under vigorous stirring to form a transparent solution. Ultrapure water was used in all the experiments. The solution was nebulized at 1.7 MHz ± 10% (YUYUE402AI, Shanghai) and then carried by air with different flow rates from 2 to 10 L·min^{-1} through a quartz tube surrounded by a furnace thermostated at 400~900°C. The quartz reaction tube with the diameter of 5.0 cm had a long length of 60 cm [25]. The products were collected in a percolator with ultrapure water and then separated by centrifugation and washed thoroughly with ethanol and ultrapure water. The products were finally dried under a vacuum at 60°C overnight. For comparison, the $Ga_{0.25}Zn_{4.67}S_{5.08}$ were prepared by a modified hydrothermal method according to the previous study [11].

2.2. Characterization. The X-ray diffraction (XRD) pattern with a scan rate of 0.05° was recorded on a Shimadzu 6100 Advance X-ray diffractometer with Cu Kα radiation in the 2θ range from 20° to 60°. Scanning electron microscopy (SEM, SU8000) was used to characterize morphology of the obtained products. Transmission electron microscopy (TEM) study was carried out on a FEI Titan G2 60-300 electron microscopy instrument. The UV-Vis diffuse reflectance spectra (UV-Vis DRS) were performed on a UV-Vis spectrophotometer (Varian, Cary 500, Palo Alto, CA, USA) with $BaSO_4$ as the reference sample in these measurements. The Brunauer-Emmett-Teller (BET) specific surface areas and porosities of the sample were carried out by using the ASAP 2020 equipment (Micromeritics, Atlanta, GA, USA). X-ray photoelectron spectroscopy (XPS) measurements were performed on a PHI Quantum 2000 XPS system (Physical Electronics, Portland, OR, USA); all the binding energies were calibrated to the C 1s peak at 284.8 eV of the surface adventitious carbon. Photocurrent was measured by an electrochemical workstation (Multi Autolab M20) in a three-electrode system with a working electrode, a Pt sheet counter electrode, and a standard Ag/AgCl reference electrode containing 0.2 mol·L^{-1} Na_2SO_4 solution as the electrolyte.

2.3. Photocatalytic Antibacterial Tests. The experiments of photocatalytic disinfection were carried out by using a 300 W Xe lamp with a UV cutoff filter (800 nm ≥ λ ≥ 420 nm) as the light source. All glassware and 0.9% saline were autoclaved at 121°C for 20 min before the experiments. Typically, 10 mg of nanocrystal powder was mixed with 50 mL saline in the quartz cell, followed by the addition to 1 mL of the suspension containing *E. coli* cells. The suspension was stirred in darkness for 1 h to achieve adsorption equilibrium of viruses on the photocatalyst. Then, at different time intervals, 0.1 mL of the reaction mixture was collected and immediately diluted with sterilized saline for a serial dilution. Following that, 0.1 mL of the diluted solution was spread uniformly on nutrient agar and incubated at 37°C for 12 h; the number of viable cells was counted. The survival rate was estimated by the following equation: survival rate% = $(N_T/N_0) \times 100\%$, where N_0 and N_T are the numbers of viable cells in darkness and after photocatalytic reaction with photocatalysts, respectively.

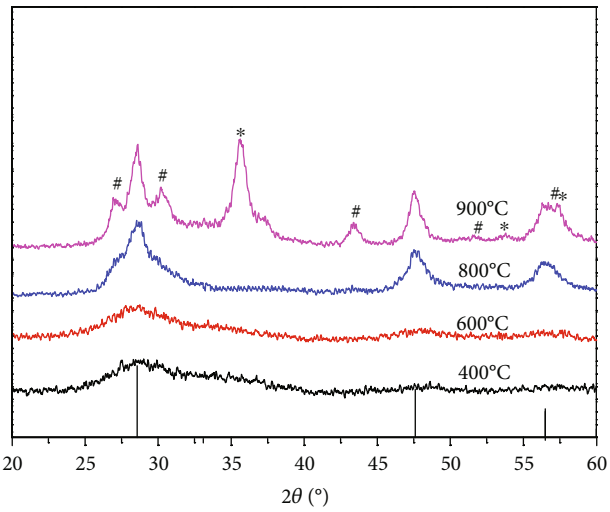

(#) ZnS
(∗) Ga_2O_3

FIGURE 1: XRD patterns of $Ga_{0.25}Zn_{4.67}S_{5.08}$ prepared at different temperatures.

3. Result and Discussion

The X-ray powder diffraction analysis result is shown in Figure 1. The diffraction peaks at 28.6°, 47.6°, and 56.5° correspond to the (111), (220), and (311) planes of the cubic structure of $Ga_{0.25}Zn_{4.67}S_{5.08}$ (JCPDS card 49-1626), respectively. Among all of the peaks, the diffraction peak at (111) gradually becomes more intense and narrow with pyrolysis temperature, suggesting an increasing degree of crystallinity [26, 27]. At the same time, these synthesized samples prepared at 400°C and 600°C have a wide diffraction peak, indicating that the samples have smaller crystals and possibly improved the catalytic efficiency. The average grain sizes calculated by the Scherrer equation of the samples prepared at 400, 600, and 800°C are 1.03, 1.32, and 3.18 nm, respectively [28]. Nevertheless, when the temperature rises to 900°C, there are some possible Ga_2O_3 and ZnS impurity diffraction peaks in the XRD pattern, which may be due to the oxidation and decomposition of $Ga_{0.25}Zn_{4.67}S_{5.08}$ caused by high temperature.

Figures 2(a)–2(c) show the SEM images of the samples fabricated at 400°C and 800°C, respectively. It can be seen from Figure 2(a) that the samples were composed of well-defined spherical microspheres, and their diameters are approximately distributed between 100 nm and 1200 nm. By comparing with Figures 2(b) and 2(c), it can be found that there is a rough surface of the sample prepared at 400°C, which will increase the specific surface area and the active sites in the photocatalytic process, eventually leading to the enhancement of photocatalytic activity. When the temperature was raised to 800°C, the surface of the particles becomes relatively smooth. This can be ascribed to the increase of grain size under high temperature, and the surface roughness gradually decreases.

The spherical and porous structures of the as-prepared $Ga_{0.25}Zn_{4.67}S_{5.08}$ sample were further confirmed by TEM. The TEM images in Figures 2(d)–2(f) illustrate that the $Ga_{0.25}Zn_{4.67}S_{5.08}$ sample has porous structured microspheres and was built by the aggregation of plenty of nanoparticles. This structure will be beneficial to increase the specific surface area and the surface active sites of the catalyst. By enabling more contacts of the pollutant molecules with the catalysts, the performance in the photocatalytic process is thus improved. The composition of the product was confirmed by EDX analysis (Figure 2(g)), proving the presence of Ga, Zn, and S in the as-prepared sample.

On the basis of the above results, an illustration of the possible three-stage formation mechanism of $Ga_{0.25}Zn_{4.67}S_{5.08}$ microspheres was suggested (Scheme 1). First, the solution was atomized into aerosol under ultrasonic conditions. The aerosols were then carried by air through the quartz tube surrounded by a furnace. Subsequently, the droplets were rapidly vaporized under high temperature, while the thiourea in the aerosol also decomposes quickly and produces H_2S. The produced H_2S rapidly reacted with the metal precursor to form ternary sulfide submicrospheres, while the mass and heat transfer were accelerated under gasification conditions. As the droplets were further evaporated and concentrated, the particle size gradually reduced to the obtained spherical particles.

The optical absorption properties of $Ga_{0.25}Zn_{4.67}S_{5.08}$ calcined at different temperatures were characterized by diffuse reflectance UV-Vis spectra (DRS) in the range of 200~800 nm as shown in Figure 3(a). All the samples display remarkable absorption in the visible region. Besides, the blue shift of the absorption band edge can be observed when the preparation temperature decreases from 900°C to 400°C. The blue shift of the adsorption edge with the decrease in preparation temperature is mainly due to the quantum confinement effect [26]. The energy band gap (E_g) of the sample can be calculated by the formula $\alpha h\nu = A(h\nu - E_g)^n$ [29]. The band gaps of the catalysts prepared at 400, 600, 800, and 900°C are calculated to be 2.21, 2.52, 2.45, and 2.29 eV, respectively, which indicates that the synthesized samples can respond well to visible light.

The chemical states of elements for the $Ga_{0.25}Zn_{4.67}S_{5.08}$ prepared at 600°C were examined by XPS analysis. The wide scan XPS spectrum (Figure 4(a)) reveals that the predominant elements are C, O, S, Zn, and Ga. Among these elements, S, Zn, and Ga elements are from the prepared composites, while C and O elements are from the XPS instrument itself and the adsorbed hydroxyl groups, respectively. The high-resolution spectra of the Ga 2p with two characteristic peaks at 1117.8 eV and 1144.6 eV corresponded to the $2p_{3/2}$ and $2p_{1/2}$ levels (Figure 4(b)), suggesting the existence of Ga^{3+} species [30]. As shown in Figure 4(c), the two peaks at the binding energies of 161.4 eV and 162.6 eV can be attributed to the $2p_{3/2}$ and $2p_{1/2}$ levels of S^{2-} [31]. The binding energies of two major peaks at 1021.0 eV and 1044.0 eV ascribed to Zn $2p_{3/2}$ and for $2p_{1/2}$, respectively (Figure 4(d)), in accordance with Zn^{2+} in $Ga_{0.25}Zn_{4.67}S_{5.08}$ [32]. These results further indicate that $Ga_{0.25}Zn_{4.67}S_{5.08}$ can be successfully synthesized via USP.

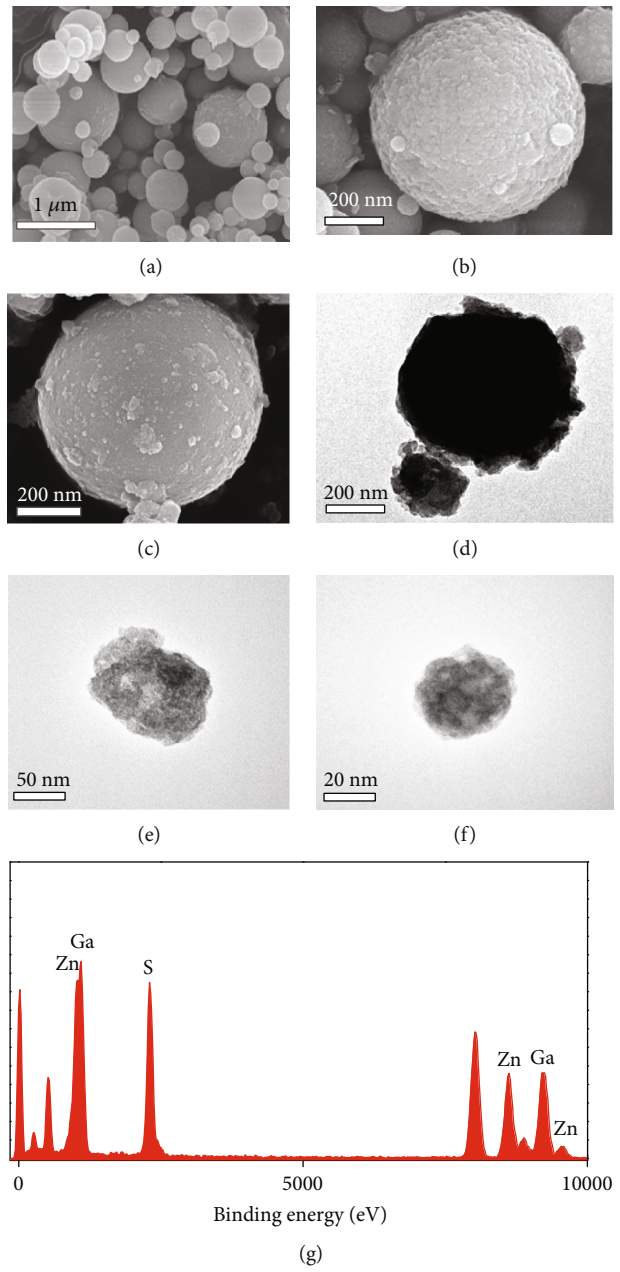

Figure 2: SEM images, TEM image, and energy dispersive spectrum of $Ga_{0.25}Zn_{4.67}S_{5.08}$ at different temperatures: (a, b) 400°C SEM images; (c, f) 800°C SEM images; (d, e) 400°C TEM images; (g) 400°C EDX spectrum.

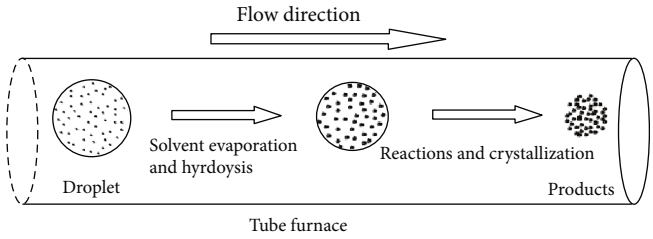

Scheme 1: Schematic diagram of the formation of $Ga_{0.25}Zn_{4.67}S_{5.08}$ microsphere.

The nitrogen adsorption-desorption isotherms and pore size distribution curve of the as-prepared samples were depicted in Figure 5. As shown in Figure 5(a), the physical adsorption isotherms of all the samples show the typical type IV isotherms with H3 hysteresis loop. The pore size obtained from the desorption branch of the isotherms exhibits a

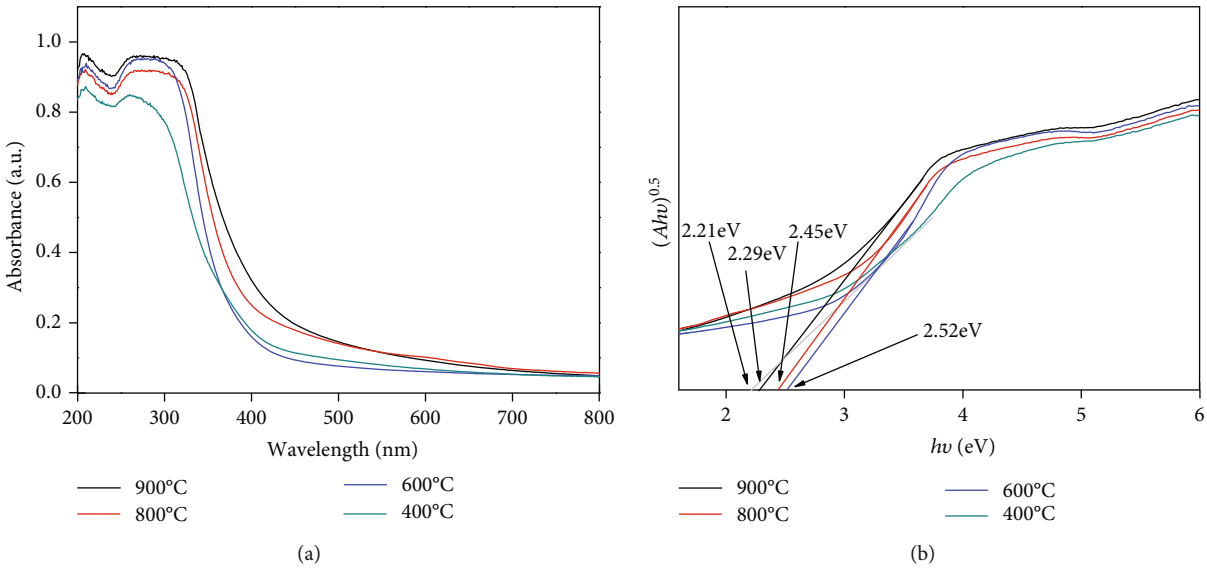

FIGURE 3: (a) Diffuse reflectance UV-Vis spectra of $Ga_{0.25}Zn_{4.67}S_{5.08}$ prepared at different temperatures; (b) the plot of the transformed Kubelka-Munk function versus the energy of light.

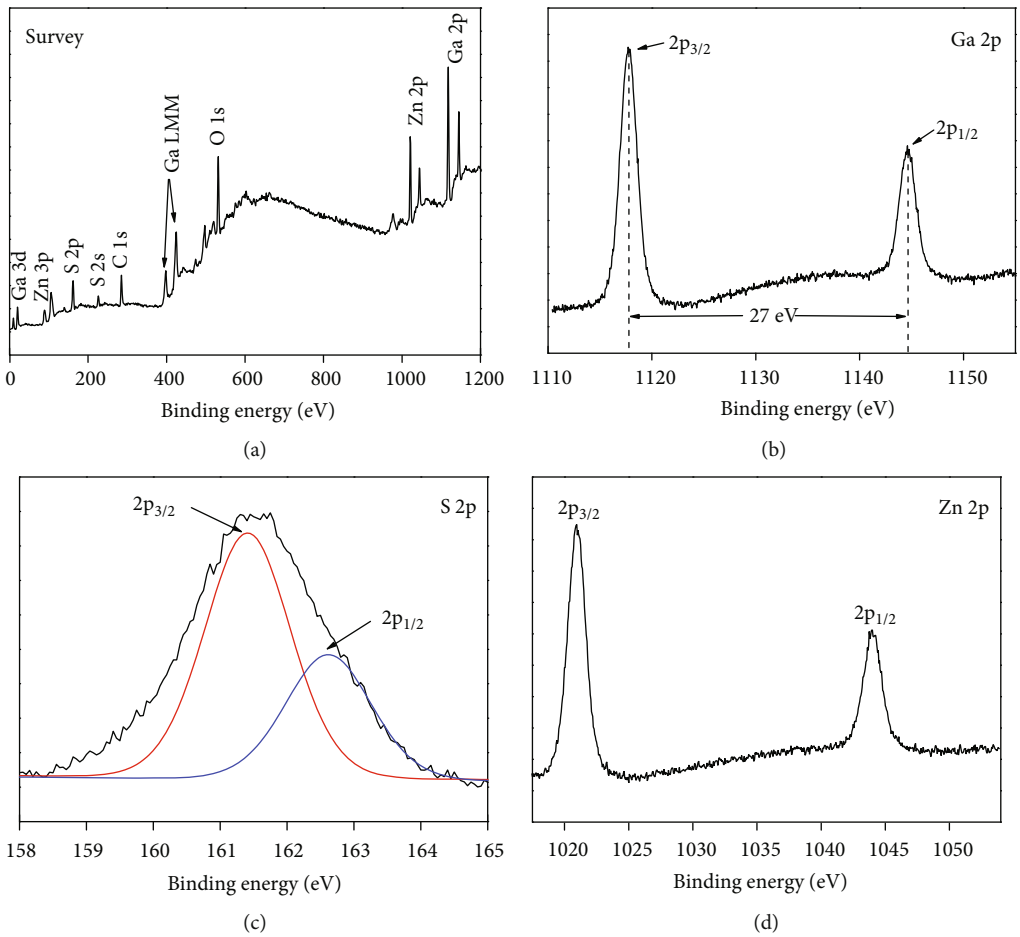

FIGURE 4: XPS spectra of catalyst prepared at 600°C: (a) the wide spectrum; (b) Ga 2p; (c) S 2p; (d) Zn 2p.

narrow distribution in the range of from 2 to 10 nm (Figure 5(b)), indicating the mesoporous nature of the as-prepared sample [33]. The porous structures with high specific surface areas could adsorb more active species and reactants on its surface and provide efficient transport pathways for the reactants and products during the photocatalytic

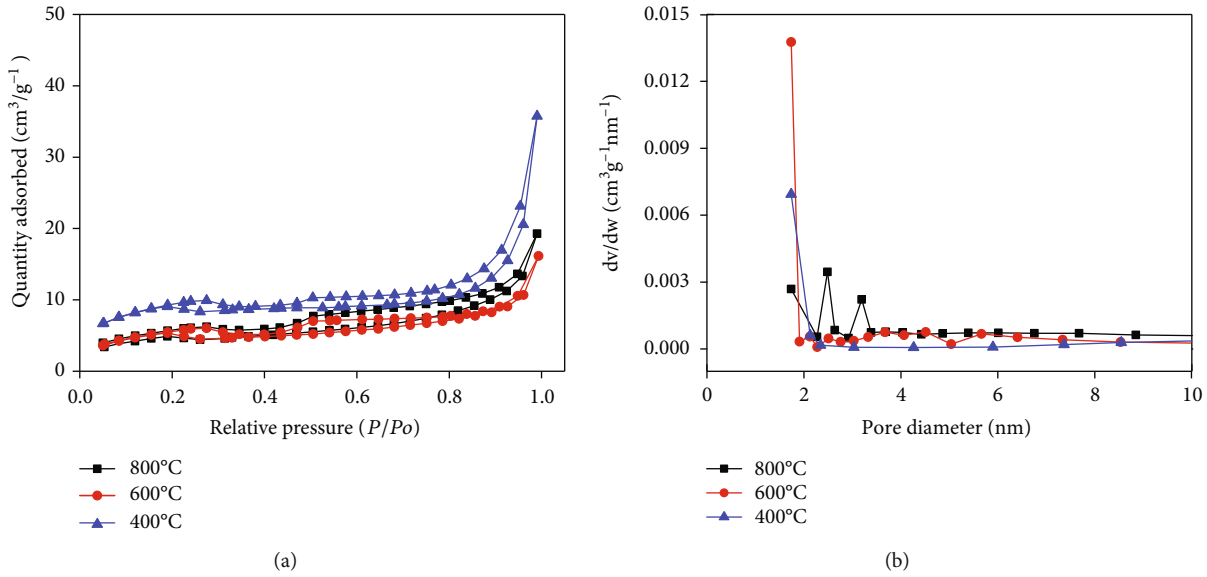

Figure 5: (a) N_2 adsorption-desorption isotherms; (b) pore size distribution curves of catalysts prepared at different temperatures.

Table 1: Porous properties of catalysts prepared at different temperatures.

Temperature (°C)	d (nm)	Pore size (nm)	Surface area ($m^2 \cdot g^{-1}$)	Pore volume ($cm^3 \cdot g^{-1}$)
400	1.03	13.85	25.76	0.05
600	1.32	7.69	13.91	0.02
800	3.18	7.40	14.00	0.03

process, thus accelerating the photocatalytic reaction rate. The BET surface areas of the $Ga_{0.25}Zn_{4.67}S_{5.08}$ prepared at 400, 600, and 800°C were 25.76, 13.91, and 14.00 $m^2 \cdot g^{-1}$, respectively (Table 1). The catalyst prepared at 400°C possesses the highest specific surface area and the largest average pore size of 13.85 nm, compared with that of samples prepared at 600°C and 800°C at 7.69 and 7.40 nm, respectively.

Efficient charge separation is also an important factor affecting photocatalytic performance [34]. The photocurrent response as a useful method to evaluate the charge separation was tested. As shown in Figure 6, all samples have great photoelectric performance, manifesting that they could respond to visible light. Obviously, photocurrent generation was shown to be affected by the calcined temperature. Notably, the photocurrent of the sample obtained at 400°C is higher than that of the samples obtained at 600°C and 800°C, which could be ascribed to the fact that the sample obtained at 400°C has a larger specific surface area and more surface active sites. As a result, much more photogenerated electrons and holes can be produced. The photocurrent density generated by the 800°C sample was higher than that of the 600°C sample, which can be ascribed to the fact that the sample prepared at higher temperature has a higher crystallinity. The higher crystallinity may decrease the electron-hole pair recombination rate and lead to higher photocurrent density. The falling edges also show that the lifetime of the photogenerated carriers of the samples prepared at 400°C is much longer than that of 600°C and 800°C, which indicates that the

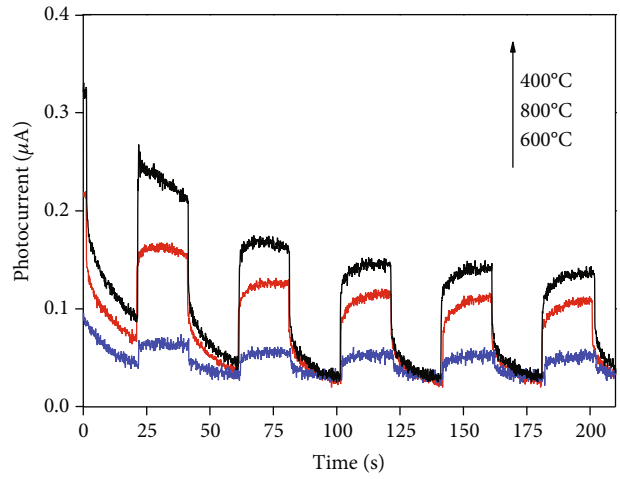

Figure 6: Photocurrent of $Ga_{0.25}Zn_{4.67}S_{5.08}$ prepared at different temperatures.

recombination of carriers of the samples prepared at 400°C is much lower than that of 600°C and 800°C. This is also benefit to photocatalytic performance.

The photocatalytic performances of the as-prepared $Ga_{0.25}Zn_{4.67}S_{5.08}$ samples with different temperatures were evaluated by measuring the survival rate of *E. coli* under visible light irradiation. As shown in Figure 7, no evident loss of survival rate was observed in the dark, indicating negligible toxicity of the photocatalyst. For the light control

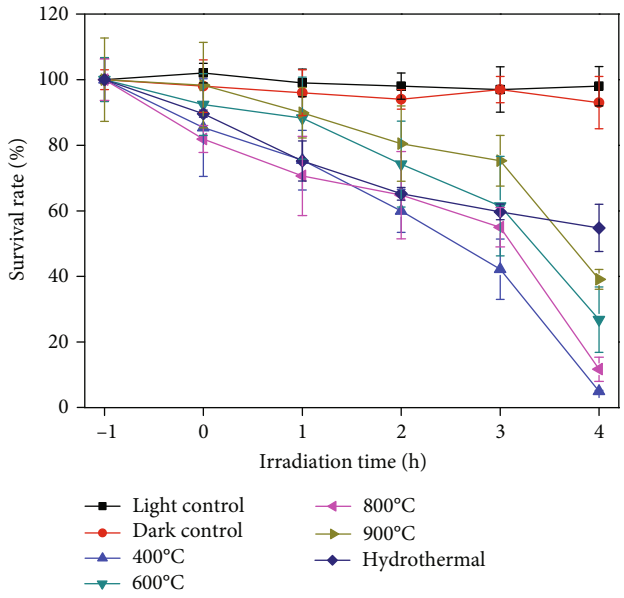

Figure 7: Disinfection efficiencies of $Ga_{0.25}Zn_{4.67}S_{5.08}$ prepared at different temperatures and hydrothermal method.

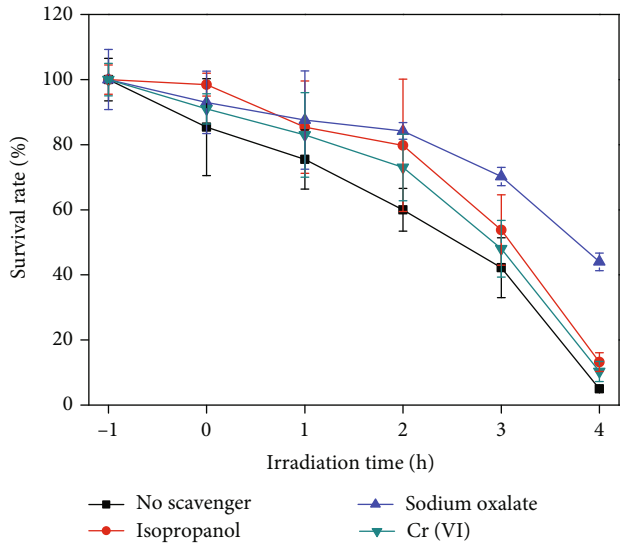

Figure 8: Disinfection efficiencies of catalysts in the presence of different sacrificial agents.

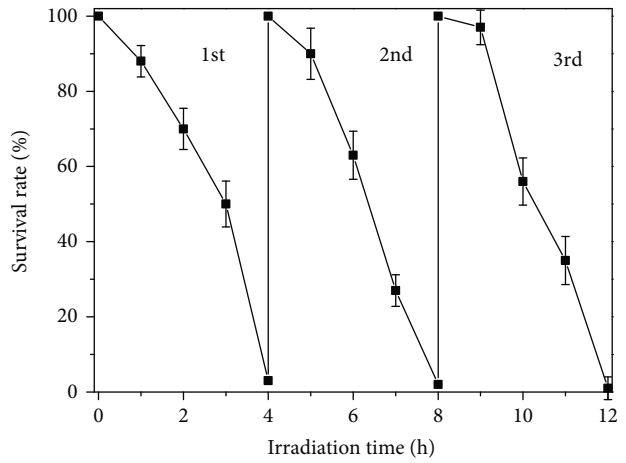

Figure 9: Stability of $Ga_{0.25}Zn_{4.67}S_{5.08}$ prepared at 400°C under visible light irradiation.

experiment, the test was performed without photocatalyst under the irradiation of visible light. The survival rate is stable which indicates the *E. coli* cannot be killed by visible light under the present condition. For the photocatalytic test, the suspension was stirred in darkness for 1 h to achieve adsorption equilibrium of the cells on the photocatalyst. As observed, all samples prepared by USP have greater bactericidal performance, compared to the sample prepared by the hydrothermal method. Under the presence of $Ga_{0.25}Zn_{4.67}S_{5.08}$ (400°C), nearly all bacteria cannot survive after 4 h of visible light irradiation, while the survival rate of other samples (600°C and 800°C) was only 27% and 12%, respectively. The bacterial suspension after the reaction was cultured for 96 h under dark reaction, and no change in the colony of *E. coli* was observed, indicating that the bacteria were indeed killed by the photocatalytic sterilization process, rather than simply suppressed. The higher photocatalytic performance of $Ga_{0.25}Zn_{4.67}S_{5.08}$ (400°C) can be ascribed to its larger specific surface area and more active sites.

It is well known that active groups such as $^{\bullet}OH$, e^-, and h^+ attack the bacterial cells during the reaction, eventually causing the decomposition of the cell wall [1]. In order to further explore which active substance played a decisive role in the photocatalytic sterilization process, different kinds of radical scavengers were added to a series of identical photocatalytic reaction systems. For example, sodium oxalate (0.5 mM as h^+ quencher), Cr (VI) (0.05 mM as e^- quencher), and isopropanol (0.5 mM as OH quencher) are added to the different batches of the $Ga_{0.25}Zn_{4.67}S_{5.08}$ photocatalytic system, respectively, to capture h^+, e^-, and $^{\bullet}OH$ and to ensure that the scavengers under the concentration will not have any toxicity to *E. coli* [35]. As shown in Figure 8, the bacterial survival rate of photocatalytic systems added with isopropanol or Cr (VI) is almost the same with the system without a trapping agent, suggesting that $^{\bullet}OH$ and e^- are not the main active substances in the photocatalytic sterilization, whereas when sodium oxalate was added as the hole trapping agent, the survival rate of bacteria reached 45% after irradiation for 4 h, suggesting that h^+ oxidation was the dominant radical for the photocatalytic disinfection.

The stability of the samples was evaluated by successive cycles of the photocatalytic sterilization process. As shown in Figure 9, the results indicate that the photocatalytic activity of the sample did not decrease significantly even after three successive cycles. These results indicate that $Ga_{0.25}Zn_{4.67}S_{5.08}$ microspheres possess excellent photocatalytic stability during the photocatalytic application.

Based on the above experimental and characterization results, a possible photocatalytic mechanism for disinfection by $Ga_{0.25}Zn_{4.67}S_{5.08}$ microspheres was proposed and displayed in Figure 10. Under the visible light irradiation, the hole and electron pairs are generated and separated; then,

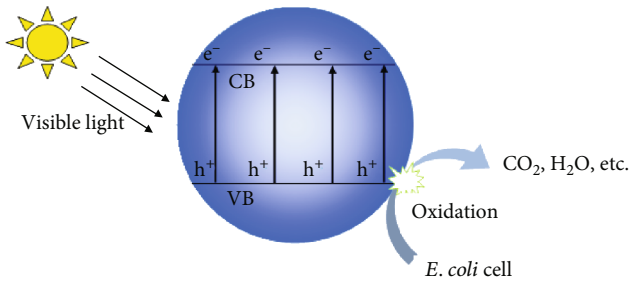

FIGURE 10: Proposed mechanism for disinfection over $Ga_{0.25}Zn_{4.67}S_{5.08}$ under visible light irradiation.

the holes directly reacted with the cells adsorbed and produce inorganic matters.

4. Conclusion

In summary, $Ga_{0.25}Zn_{4.67}S_{5.08}$ microspheres were synthesized by the USP process without adding template. The visible light photocatalytic antibacterial results indicate that the temperature of pyrolysis plays a dominant role in the disinfection process. On the basis of the DRS and BET, as well as the photocurrent, the superior photocatalytic activity of $Ga_{0.25}Zn_{4.67}S_{5.08}$ prepared at 400°C was ascribed to the narrowed band gap, the high specific surface areas, and more photogenerated holes. We believe that this study shed light on engineering other novel porous structured photocatalysts for low-cost water disinfection.

Data Availability

The data used to support the findings of this study are available from the corresponding author upon request.

Conflicts of Interest

The authors declare that they have no conflicts of interest.

Acknowledgments

This work was supported by the Natural Science Foundation of Fujian Province (Grant No. 2016J05042), the Putian Science and Technology Bureau Project (2016S1001), and the Putian University Research Innovation Project (2018ZP03 and 2018ZP07) and the Putian University Research Project (2018048).

References

[1] Y. Zhang, C. Lin, Q. Lin et al., "CuI-BiOI/Cu film for enhanced photo-induced charge separation and visible- light antibacterial activity," *Applied Catalysis B: Environmental*, vol. 235, pp. 238–245, 2018.

[2] Y. Wang, L. Lin, B. B. Li, M. H. Huang, B. B. Li, and L. Chen, "Preparation of hierarchical microsphere BiOBr catalyst and its photocatalytic disinfection performance under visible light," *Biotechnology Bulletin*, vol. 32, no. 8, pp. 242–248, 2016.

[3] M. G. Muellner, E. D. Wagner, K. McCalla, S. D. Richardson, Y. T. Woo, and M. J. Plewa, "Haloacetonitriles vs. regulated haloacetic acids: are nitrogen-containing DBPs more toxic?," *Environmental Science & Technology*, vol. 41, no. 2, pp. 645–651, 2007.

[4] H. Yu, S. Chen, X. Quan, and Z. Zhang, "The mechanism, materials and reactors of photocatalytic disinfection in water and wastewater treatment," *Progress in Chemistry*, vol. 29, no. 9, pp. 1030–1041, 2017.

[5] B. E. Logan and M. Elimelech, "Membrane-based processes for sustainable power generation using water," *Nature*, vol. 488, no. 7411, pp. 313–319, 2012.

[6] C. M. Zhang, Y. H. Miao, Q. P. Zhang, and H. Xu, "Effects of chlorination and ultraviolet disinfection on antibiotic resistance of fecal coliforms in secondary settling tank effluent of municipal wastewater treatment plant," *Research of Environmental Sciences*, vol. 27, no. 4, pp. 422–426, 2014.

[7] L. Jia, H. Xiangfeng, S. Jie, and W. Zhichao, "Controlling photo-reactivation of bacteria inactivated by UV disinfection," *Environmental Pollution & Control*, vol. 29, no. 11, pp. 841–843, 2007.

[8] T. V. M. Sreekanth, P. C. Nagajyothi, P. Muthuraman et al., "Ultra-sonication-assisted silver nanoparticles using _Panax ginseng_ root extract and their anti-cancer and antiviral activities," *Journal of Photochemistry and Photobiology B-Biology*, vol. 188, pp. 6–11, 2018.

[9] J. H. Huang, W. T. Lin, L. Y. Xie, and J. Q. Chen, "Construction of graphitic carbon nitride-bismuth oxyiodide layered heterostructures and their photocatalytic antibacterial performance," *Environmental Science*, vol. 38, no. 9, pp. 3979–3986, 2017.

[10] H. L. Tan, R. Amal, and Y. H. Ng, "Alternative strategies in improving the photocatalytic and photoelectrochemical activities of visible light-driven $BiVO_4$: a review," *Journal of Materials Chemistry A*, vol. 5, no. 32, pp. 16498–16521, 2017.

[11] B. Poornaprakash, U. Chalapathi, S. V. P. Vattikuti et al., "Enhanced fluorescence efficiency and photocatalytic activity of ZnS quantum dots through Ga doping," *Ceramics International*, vol. 45, no. 2, pp. 2289–2294, 2019.

[12] B. Poornaprakash, U. Chalapathi, S. V. Prabhakar Vttikuti, M. S. Pratap Reddy, and S. H. Park, "Pristine and Sm-doped ZnS quantum dots: structural, optical, luminescence, magnetic, and photocatalytic properties," *Chalcogenide Letters*, vol. 16, no. 2, pp. 49–55, 2019.

[13] S. V. P. Vattikuti, C. Byon, and S. Jeon, "Enhanced photocatalytic activity of ZnS nanoparticles loaded with MoS_2 nanoflakes by self-assembly approach," *Physica B: Condensed Matter*, vol. 502, pp. 103–112, 2016.

[14] B. Poornaprakash, U. Chalapathi, P. T. Poojitha, S. V. P. Vattikuti, and S.-H. Park, "Co-doped ZnS quantum dots: structural, optical, photoluminescence, magnetic, and photocatalytic properties," *Journal of Superconductivity and Novel Magnetism*, pp. 1–6, 2019.

[15] N. Bouaniza, N. Hosni, and H. Maghraoui-Meherzi, "Structural and optical properties of Cu_3SbS_3 thin film deposited by chemical bath deposition along with the degradation of methylene blue," *Surface and Coatings Technology*, vol. 333, pp. 195–200, 2018.

[16] Y. Chen, R. Huang, D. Chen et al., "Exploring the different photocatalytic performance for dye degradations over hexagonal $ZnIn_2S_4$ microspheres and cubic $ZnIn_2S_4$ nanoparticles," *ACS Applied Materials & Interfaces*, vol. 4, no. 4, pp. 2273–2279, 2012.

[17] X. Hong, Q. Liu, J. Iocozzia et al., "Needle-leaf-like Cu2Mo6S8Films for highly efficient visible-light photocatalysis," *Particle & Particle Systems Characterization*, vol. 35, no. 1, article 1700302, 2018.

[18] M. A. Yewale, A. K. Sharma, D. B. Kamble, C. A. Pawar, S. S. Potdar, and S. C. Karle, "Electrochemical synthesis of CuS_xSe_{1-x} thin film for supercapacitor application," *Journal of Alloys and Compounds*, vol. 754, pp. 56–63, 2018.

[19] Q. Liu, X. Hong, X. Zhang et al., "Hierarchical Cu_2S nanorods with different crystal phases for asymmetrical supercapacitors and visible-light photocatalysis," *Dalton Transactions*, vol. 47, no. 42, pp. 15189–15196, 2018.

[20] I. Caraman, S. Evtodiev, D. Untila et al., "Optical and photoelectric properties of planar structures obtained by thermal annealing of Ga2S3Plates in Zn vapors," *physica status solidi (a)*, vol. 214, no. 12, article 1700808, 2017.

[21] M. Gusain, A. Dubey, M. Das, and S. K. Singh, "Facial surfactant-free hydrothermal synthesis of MoS_2 microflower and its effect in electrochemical properties," *Journal of Solid State Chemistry*, vol. 274, pp. 58–63, 2019.

[22] S. Z. Werta, O. K. Echendu, and F. B. Dejene, "Optical and morphological studies of electrodeposited CdS thin film grown at different deposition times from acetate precursor," *ECS Journal of Solid State Science and Technology*, vol. 8, no. 2, pp. P112–P118, 2019.

[23] C. Nethravathi, R. Ragesh Nath, J. T. Rajamathi, and M. Rajamathi, "Microwave-assisted synthesis of porous aggregates of CuS nanoparticles for sunlight photocatalysis," *ACS Omega*, vol. 4, no. 3, pp. 4825–4831, 2019.

[24] A. A. G. Santiago, L. X. Lovisa, P. N. Medeiros et al., "Fast and simultaneous doping of $Sr_{0.9-x-y-z}Ca_{0.1}In_2O_4$:(xEu(3+), yTm(3+), zTb(3+)) superstructure by ultrasonic spray pyrolysis," *Ultrasonics Sonochemistry*, vol. 56, pp. 14–24, 2019.

[25] N. Gajić, Ž. Kamberović, Z. Anđić, J. Trpčevská, B. Plešingerova, and M. Korać, "Synthesis of tribological WS_2 powder from WO_3 prepared by ultrasonic spray pyrolysis (USP)," *Metals*, vol. 9, no. 3, p. 277, 2019.

[26] J. Huang, W. Lin, and J. Chen, "Synthesis of CdIn $_{**2**}$ S $_{**4**}$ Microsphere and Its Photocatalytic Activity for Azo Dye Degradation," *The Scientific World Journal*, vol. 2014, Article ID 241234, 6 pages, 2014.

[27] L. Lin, W. Ren, C. Wang, A. M. Asiri, J. Zhang, and X. Wang, "Crystalline carbon nitride semiconductors prepared at different temperatures for photocatalytic hydrogen production," *Applied Catalysis B: Environmental*, vol. 231, pp. 234–241, 2018.

[28] M. A. Subhan, P. C. Saha, P. Sarker, and M. al-Mamun, "Photoluminescence and enhanced visible light driven photocatalysis studies of MoO_3·CuO·ZnO nanocomposite," *Research on Chemical Intermediates*, vol. 44, no. 10, pp. 6311–6326, 2018.

[29] P. Li, H. Hu, J. Xu et al., "New insights into the photo-enhanced electrocatalytic reduction of carbon dioxide on MoS_2-rods/TiO_2 NTs with unmatched energy band," *Applied Catalysis B: Environmental*, vol. 147, pp. 912–919, 2014.

[30] Y. Pan, L. Wang, S. Li, D. W. Gao, and X. W. Han, "Preparation and characterization of Co and Ga_2O_3-codoped ZnS and ZnSe bulk ceramics," *RSC Advances*, vol. 7, no. 80, pp. 50928–50934, 2017.

[31] C. Zeng, H. Huang, T. Zhang, F. Dong, Y. Zhang, and Y. Hu, "Fabrication of heterogeneous-phase solid-solution promoting band structure and charge separation for enhancing photocatalytic CO_2 reduction: a case of Zn_XCa_1-XIn_2S_4," *ACS Applied Materials & Interfaces*, vol. 9, no. 33, pp. 27773–27783, 2017.

[32] S. Y. Chae, S. J. Park, S. G. Han et al., "Enhanced photocurrents with ZnS passivated Cu(In,Ga)(Se,S)2Photocathodes synthesized using a nonvacuum process for solar water splitting," *Journal of the American Chemical Society*, vol. 138, no. 48, pp. 15673–15681, 2016.

[33] J. Liu, S. Zhang, and H. Zhao, "Fabricating visible-light photoactive 3D flower-like BiOCl nanostructures via a one-step solution chemistry method at room temperature," *Applied Surface Science*, vol. 479, pp. 247–252, 2019.

[34] W. H. Zhang, Q. H. Ji, H. C. Lan, and J. Li, "Preparation of $ZnTiO_3$/TiO_2 photocatalyst and its mechanism on photocatalytic degradation of organic pollutants," *Environmental Science*, vol. 40, no. 2, pp. 693–700, 2019.

[35] W. Wang, Y. Yu, T. An et al., "Visible-light-driven photocatalytic inactivation of E. coli K-12 by bismuth vanadate nanotubes: bactericidal performance and mechanism," *Environmental Science & Technology*, vol. 46, no. 8, pp. 4599–4606, 2012.